Title

Validation of an automated technique for quantification of pulmonary perfusion territories using computed tomography angiography.

Journal

Quantitive Imaging in Medicine and Surgery, 13(5)

ISSN

2223-4292

Authors

Zhao, Yixiao

Malkasian, Shant

Hubbard, Logan

et al.

Publication Date

2023-05-01

DOI

10.21037/qims-22-791

Peer reviewed

Original Article

Validation of an automated technique for quantification of pulmonary perfusion territories using computed tomography angiography

Yixiao Zhao^, Shant Malkasian^, Logan Hubbard^, Sabee Molloi

Department of Radiological Sciences, Medical Sciences I, B-140, University of California, Irvine, CA, USA

Contributions: (I) Conception and design: All authors; (II) Administrative support: S Molloi; (III) Provision of study materials or patients: S Molloi; (IV) Collection and assembly of data: Y Zhao, L Hubbard, S Malkasian; (V) Data analysis and interpretation: Y Zhao, L Hubbard, S Malkasian; (VI) Manuscript writing: All authors; (VII) Final approval of manuscript: All authors.

Correspondence to: Sabee Molloi, PhD. Department of Radiological Sciences, Medical Sciences I, B-140, University of California, Irvine, CA 92697, USA. Email: symolloi@uci.edu.

Background: Computed tomography pulmonary angiography (CTPA) is the primary modality for the detection and diagnosis of pulmonary embolism (PE) while the stratification of PE severity remains challenging using angiography. Hence, an automated minimum-cost path (MCP) technique was validated to quantify the subtended lung tissue distal to emboli using CTPA.

Methods: A Swan-Ganz catheter was placed in the pulmonary artery of seven swine (body weight: 42.6±9.6 kg) to produce different PE severities. A total of 33 embolic conditions were generated, where the PE location was adjusted under fluoroscopic guidance. Each PE was induced by balloon inflation followed by computed tomography (CT) pulmonary angiography and dynamic CT perfusion scans using a 320-slice CT scanner. Following image acquisition, the CTPA and the MCP technique were used to automatically assign the ischemic perfusion territory distal to the balloon. Dynamic CT perfusion was used as the reference standard (REF) where the low perfusion territory was designated as the ischemic territory. The accuracy of the MCP technique was then evaluated by quantitatively comparing the MCP-derived distal territories to the perfusion-derived reference distal territories by mass correspondence using linear regression, Bland-Altman analysis, and paired sample *t*-test. The spatial correspondence was also assessed.

Results: The MCP-derived distal territory masses ($Mass_{MCP}$, g) and the reference standard ischemic territory masses ($Mass_{REF}$, g) were related by $Mass_{MCP} = 1.02 Mass_{REF} - 0.62$ g (r=0.99, paired *t*-test P=0.51). The mean Dice similarity coefficient was 0.84±0.08.

Conclusions: The MCP technique enables accurate assessment of lung tissue at risk distal to a PE using CTPA. This technique can potentially be used to quantify the fraction of lung tissue at risk distal to PE to further improve the risk stratification of PE.

Keywords: Computed tomography (CT); pulmonary embolism; CT angiography (CTA)

Submitted Jul 28, 2022. Accepted for publication Dec 21 2022. Published online Feb 16, 2023.
doi: 10.21037/qims-22-791
View this article at: https://dx.doi.org/10.21037/qims-22-791

^ ORCID: Yixiao Zhao, 0000-0002-8471-2309; Shant Malkasian, 0000-0002-6478-4321; Logan Hubbard, 0000-0003-2238-5768.

Introduction

Pulmonary emboli (PE) are responsible for approximately 100,000 deaths per year in the United States; the third leading cause of cardio-pulmonary related death (1-3). Owing to its high accuracy, broad availability, low invasiveness, and rapid scan time, computed tomography pulmonary angiography (CTPA) is the primary modality for diagnosis of acute PE (4,5). Nevertheless, the death rate of PE remains 8–15% (6,7); i.e., proper stratification of PE severity continues to be a challenge (8).

The implementation of multi-detector CTPA in clinical practice have improved the visualization of peripheral vessels, leading to a higher sensitivity of PE diagnosis and higher rate of subsegmental PE detection (2 to 3 mm in diameter) (9). While the rate of the subsegmental PE diagnosis is increasing with advancements of multi-detector CT (10), the true incidence of subsegmental PE remains unclear. The increase in the incidence of PE could also be the overdiagnosis or misdiagnosis by the CPTA as compared to the ventilation-perfusion (V/Q) scan that usually underdiagnoses subsegmental PEs (11). In addition, the chronic thromboembolic pulmonary hypertension (CTEPH) also has a complex pathophysiology, which involves not only persistent organized thrombus in proximal pulmonary arteries, but also extensive small-vessel diseases (12). Specifically, small-vessel abnormalities may contribute to hemodynamic compromise and functional impairment, leading to progressive pulmonary vascular disease if untreated (12,13). The degree of small-vessel disease may have a substantial impact on the severity of CTEPH and post-treatment outcomes. Given this variability in the certainty of subsegmental PE diagnosis, it is important to have quantitative CTPA results to characterize the severity of the PE for the use of optimal treatment modalities. It would be helpful to quantify the fraction of lung tissue at risk so it could be compared with the risk of anticoagulant therapy. Hence, an alternative solution for determining the clinical significance of small-vessel PE is absolutely needed to better guide medical management and further reduce PE mortality.

Several obstructive indices have been used to describe the degree of obstruction of the pulmonary emboli, such as the Miller index, Walsh index, and Qanadli index (14-17). In addition, the right-to-left ventricle size ratio is commonly used as a prognostic indictor, while it is only critical in helping to delineate massive from sub-massive PE (4,18,19). The right ventricular dysfunction is generally not observed for pulmonary arterial obstructions less than 40% (20). Unfortunately, none of these CT indexes can automatically quantify the severity of subsegmental PEs. The minimum-cost path (MCP) technique can be used to provide the spatial correspondence between the arterial tree downstream from a PE and the subtended ischemic or infarcted tissue (21,22). With the MCP technique, the total mass of lung tissue subtended to a PE can be quantified using the standard CTPA data. Hence, the subtended lung tissue at-risk can potentially be used to automatically stratify the PE severity using the CTPA without additional radiation dose.

The purpose of this study was to validate an automated MCP technique to enable accurate assignment of the subtended lung tissue distal to a PE using CTPA data. The central hypothesis was that the tissue territory distal to a PE can be accurately calculated by using the dynamic CT perfusion-derived ischemic territory as the reference standard (REF).

Methods

General methods

The study was performed under a project protocol (No. AUP-18-191) granted by the Institutional Animal Care & Use Committee (IACUC), in compliance with institutional guidelines for the care and use of animals. Seven swine (42.6±9.6 kg, male, Yorkshire), in which a total of 33 CT measurements were used for validation of the MCP technique. All experimental data were successfully acquired between Jun 2016 and July 2018 and analyzed between Oct 2020 and Jul 2021.

Animal preparation

The animals were premedicated with intramuscular injection of Telazol (4.4 mg/kg), Ketamine (2.2 mg/kg), and Xylazine (2.2 mg/kg), intubated (Mallinckrodt, tube 6.0–7.0, Covidien, Mansfield, MA, USA), then ventilated (Surgivet, Norwell, MA, USA, and Highland Medical Equipment, Temecula, CA, USA) with 1.5–2.5% Isoflurane (Baxter, Deerfield, IL, USA) to maintain anesthesia. Each swine was monitored by electrocardiogram (ECG), mean arterial pressure (mmHg), end-tidal CO_2 (mmHg), and O_2 saturation (%) during the experiment.

Under ultrasound guidance (9L Transducer, Vivid E9, GE 145 Healthcare), four introducer sheaths (AVANTIR, Cordis Corporation, Miami Lakes, FL, USA) were placed in the left and right jugular veins, right femoral vein, and

right femoral artery. Specifically, the left jugular vein was used for intravenous contrast injection. The right femoral vein was used for intravenous fluid and drug administration. The right femoral artery sheath was used for invasive blood pressure monitoring. Under fluoroscopic guidance, a 6-Fr Swan-Ganz catheter (Edwards Lifesciences Corp., Irvine, CA, USA) was placed in a distal pulmonary artery via the right jugular vein. Several different PE severities were then generated, where the location of the catheter tip was adjusted distally to proximally, and each PE was produced using prolonged balloon inflation (balloon diameter: 2–4 mm). Upon completion of each the experiment, each animal was euthanized with KCl.

CT scanning protocol

Each animal was imaged supine and head-first with a 320-slice CT scanner (Aquilion One, Canon Medical Systems, Tustin, CA, USA), where the caudal lung region was localized within a 16-cm z-axis coverage. After each PE induction, contrast (0.5 mL/kg, Isovue 370, Bracco Diagnostics, Princeton, NJ, USA) and a saline chaser (0.25 mL/kg) were injected at a rate of 5 mL/s (Empower CTA, Acist Medical Systems, Eden Prairie, MN, USA). For each CT measurement, ventilation was paused at end inspiration and 20 ECG-gated dynamic CT volume scans were acquired at 100 kV and 200 mA (320 mm × 0.5 mm detector collimation, 320–400 mm scan field-of-view, 0.35 s rotation time). Full projection CT data were reconstructed at 75% R-R interval using an adaptive iterative dose reduction three-dimensional (3D) algorithm and a standard lung kernel FC07 (512×512 matrix, 0.5-mm slice thickness and slice interval, 320–400 mm reconstruction field-of-view). The image with maximum contrast enhancement was then used as the CTPA image for MCP analysis. Subsequent CT acquisitions were repeated at least 15-minute apart to allow for adequate contrast clearance and recirculation from the previous injection. The CT dose index (CTDI) and the dose-length product (DLP) were also collected from the dose report sheet.

MCP technique

The minimum-cost path technique is based on the assumption that the lung parenchyma is perfused by its nearest arterial tree and microvascular bed (23). The MCP technique was implemented to determine the minimum distance between each voxel of the lung tissue and its supplying pulmonary artery. To validate the MCP technique, a single maximally enhanced CT volume scan was selected from the dynamic volume scan series and used as the CTPA image. Next, the lung tissue and pulmonary arteries were segmented using a Vitrea workstation (Pulmonary Analysis workflow, Vitrea fX version 7.7, Vital Images, Inc., Minnetonka, MN, USA). Specifically, an automatic vessel selection tool was used for arterial segmentation followed by manual correction. The arterial centerlines and a binary mask of the lung tissue were extracted using in-house software developed in MATLAB® (R2019a; MathWorks Inc.). The MCP algorithm was then performed using the binary tissue mask with the extracted proximal and distal arterial segments (21,22). Specifically, the centerlines were used as seed points to generate distance maps through the entire lung using a Fast-Marching algorithm (24). From each distance map, the minimum-cost path from each tissue voxel to each arterial centerline was used to assign each voxel to its nearest supplying artery, resulting in the assignment of tissue for the entire lung. The Swan-Ganz balloon was visualized on CTPA and its location along the pulmonary artery centerline was manually annotated. Then, the vessel tree was split into proximal and distal segments at the midpoint of the balloon. Following assignment, the tissue mass of each territory was also estimated from the product of the total territory volume, the lung parenchymal tissue density (1.053 g/mL), and the non-air fraction of tissue (%) (25). Finally, the fraction of mass distal to each PE (PE-distal) over the entire lung mass was also computed as a percentage. The details of the MCP technique are shown in *Figure 1*.

CT perfusion technique

Dynamic CT perfusion was used to determine the reference 'perfused' or 'ischemic' territories. A previously validated two-volume, first-pass dynamic CT perfusion technique was used to calculate the pulmonary perfusion, resulting in a whole-lung 3D perfusion map in mL/min/g (25). A median filter was applied to the perfusion map, followed by automated region growing algorithm to segment out the reference 'non-ischemic' and 'ischemic' territories. Specifically, a seed point was placed within the ischemic tissue region and iteratively grown into the whole lung tissue, with a cutoff value of 3 mL/min/g for determining the boundaries of the 'ischemic' territory. As such, the entire lung volume resulted in two separate REF perfusion territories of non-ischemic and ischemic regions. The

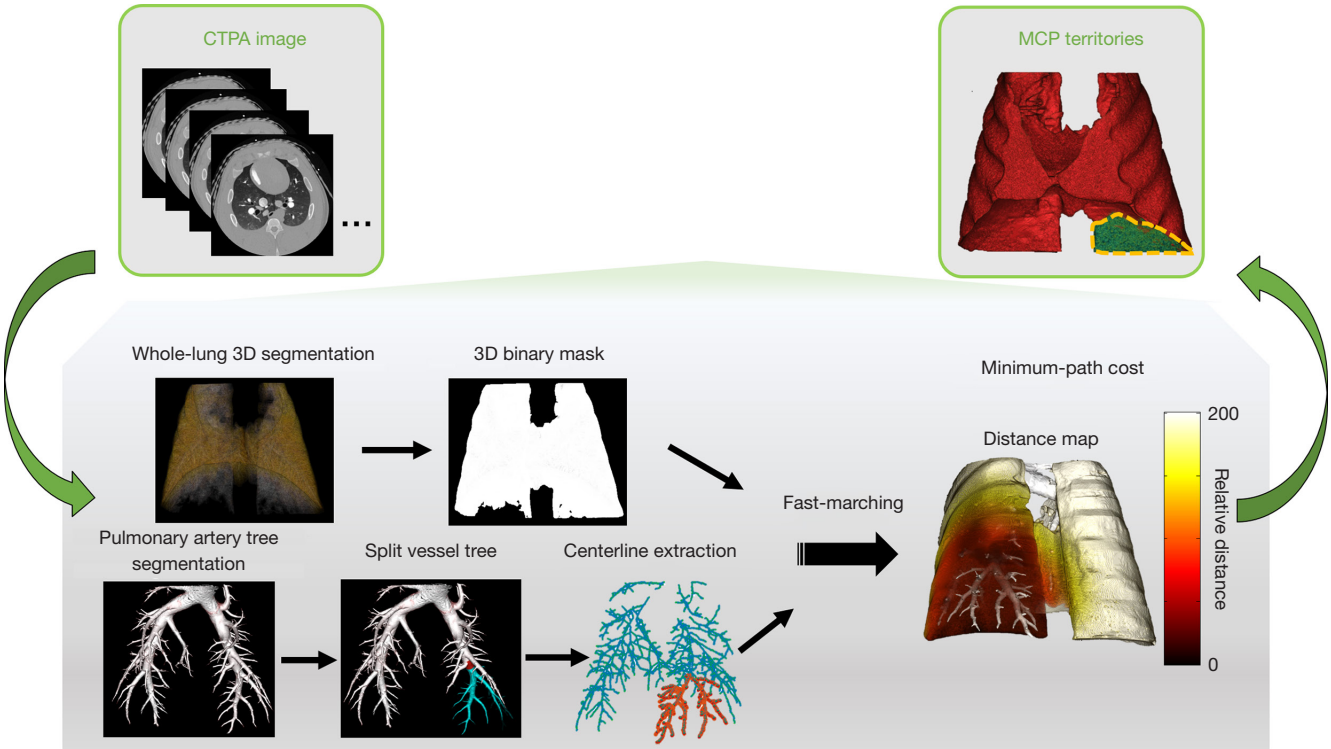

Figure 1 Minimum-cost path assignment technique. The whole-lung segmentation and the pulmonary arterial tree segmentation were performed on the CTPA image. The vessel tree was cut from the tip of the balloon location. The vessel centerlines were extracted from the vessel segmentation. Using the vessel centerlines as seed points, distance maps through a whole-lung 3D binary mask were generated using the Fast-Marching algorithm. The distance maps were used to determine the minimum-cost path of each tissue voxel to the PE-proximal and PE-distal artery subtrees, yielding MCP assignment territories. 3D, three-dimensional; CTPA, computed tomography pulmonary angiography; MCP, minimum-cost path; PE, pulmonary embolism.

REF ischemic mass and mass-percent at-risk were then calculated. The REF image processing steps are illustrated in *Figure 2*.

Evaluation metrics

Overlap-based and distance-based evaluation metrics were used for assessing the spatial correspondence between the distal MCP and REF ischemic territories (26,27). The 3D image segmentations of each paired territories were compared. First, the Dice similarity coefficient (DSC) was used for evaluating the spatial overlap between the MCP and REF territories (28,29). Specifically, the DSC computed the number of overlapping voxels divided by the total number of voxels of both volumes, ranging from 0 and 1. Second, boundary delineation was also of importance as a dissimilarity measure. The Euclidean distance was used to measure the distance between the MCP territory surface and REF territory surface in 3D. Specifically, the minimum distance was calculated for every point from one set to the nearest point in the other set, forming a distance metric. The maximum distance (MD) and average distance (AD) of the distance metric were then determined, where the MD is more sensitive to outliers than the AD. Thus, to further exclude possible outliers, the 90th percentile distance and the 50th percentile distance are reported for comparison.

Statistical analysis

The mass and spatial correspondence between the MCP-derived distal-PE territory and REF perfusion ischemic territory were compared. Statistical software (SPSS, version 22, IBM, Armonk, NY, USA) was used for all analyses. To evaluate mass correspondence, linear regression and Bland-Altman analyses were computed, along with the Pearson's r, adjusted R^2 (Adj. R^2), root-mean-square error (RMSE), root-

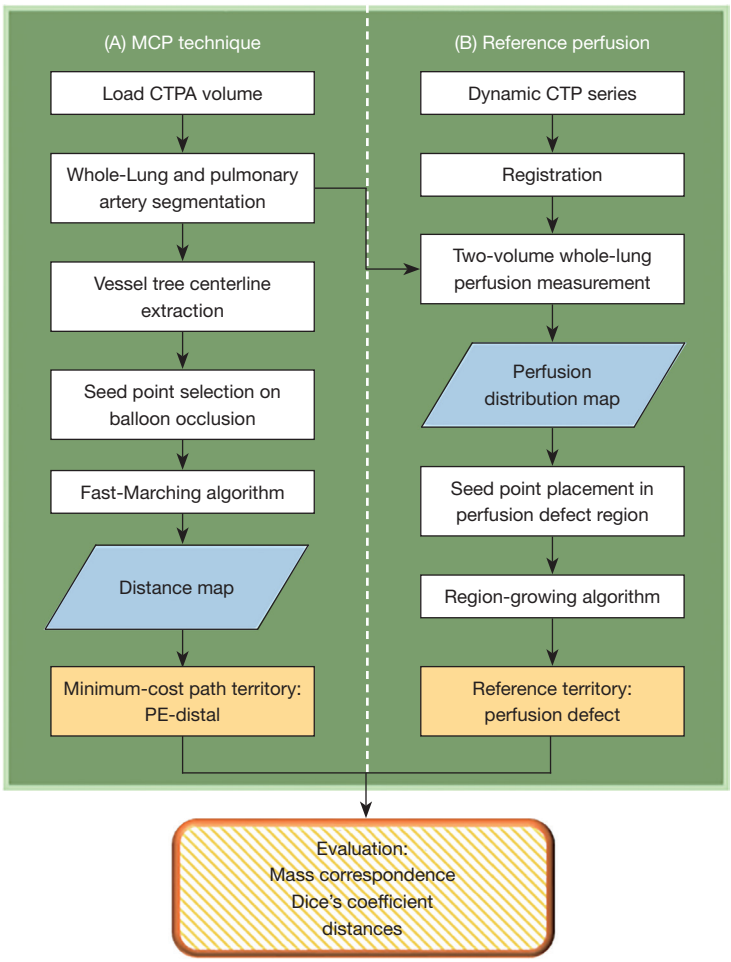

Figure 2 Image processing diagram. (A) MCP assignment processing block. The whole-lung segmentation and the pulmonary arterial tree segmentation were performed on the CTPA image. The pulmonary arterial tree was cut based on the location of the tip of the balloon. The vessel centerlines were extracted from the vessel segmentation. Using the vessel centerlines as seed points, distance maps through a whole-lung 3D binary mask were generated using the Fast-Marching algorithm. The distance maps were used to determine the MCP of each tissue voxel to the PE-proximal and PE-distal artery subtrees, yielding MCP assignment territories. (B) Reference standard processing block. Dynamic CT acquisition was performed and a first-pass perfusion technique was used to generate the perfusion distribution map. A region-growing segmentation was performed within the perfusion defect region to generate the reference standard territories. 3D, three-dimensional; CTPA, computed tomography pulmonary angiography; CTP, computed tomography perfusion; MCP, minimum-cost path; PE, pulmonary embolism.

mean-square deviation (RMSD), and Lin's concordance correlation coefficient (CCC) (30). Paired sample *t*-testing was also used to determine the mean differences between the PE-distal mass and REF ischemic mass. A histogram comparison of the mass-percent distribution of the MCP technique versus the REF data was also performed. To evaluate spatial correspondence, the Dice coefficient and Euclidean distance were computed between the MCP-derived distal-PE territory and the REF ischemic territory, including the mean DSC, AD, MD, 90th percentile distance, and 50th percentile distance.

Results

General

A total of seven swine (42.6±9.6 kg) were used for validation of the MCP technique. The average heart rate and

mean arterial pressure during all the CT acquisitions were 90.7±17.8 beats per minute and 65.4±21.4 mmHg, respectively. A total of 33 successful contrast injections and CT imaging were performed, resulting in 33 MCP-derived and REF ischemic territory pairs. The average CTDI for the single CTPA image and dynamic CT perfusion images were 4.2 and 138.7 mGy, respectively.

Qualitative performance

A representative PE for one animal is shown in *Figure 3*, demonstrating a total occlusion in the left caudal lobe. The 20-mm maximum intensity projections (MIP) of the CTPA, pulmonary perfusion maps and MCP distance maps are shown in the axial, coronal, and posterior-lateral 3D views (*Figure 3A*). The corresponding MCP PE-distal and REF ischemic territories are compared in *Figure 3B*. Further, the PE-distal tissue masses on each axial slice image are displayed for both techniques (*Figure 3C*).

Mass correspondence evaluation

The average whole-lung tissue mass was 449.9±42.6 g. The average mass of the REF ischemic territory was 47.2±35.7 g, while the average PE-distal mass of the MCP territory was 48.0±37.1 g (P=0.51, *Table 1*). Using the linear regression analysis, the MCP PE-distal territory masses ($Mass_{MCP}$, g) and the REF ischemic territory masses ($Mass_{REF}$, g) were related by $Mass_{MCP}$ =1.02$Mass_{REF}$ – 0.62 g (r=0.99), with an Adj. R^2 of 0.98, a CCC of 0.97, a RMSE of 4.78 g, and a RMSD of 4.67 g (*Figure 4A*,*4B* and *Table 2*). Moreover, *Figure 4C* shows mass-percent of ischemic tissue for all PE conditions, where the number of different PE severity levels are compared between the REF and MCP techniques.

Spatial correspondence evaluation

Overall, the mean DSC of all PE conditions is 0.84±0.08. The AD, MD, 90th percentile distance, and 50th percentile distance between the distal MCP territories and REF ischemic territories were 2.12±1.03, 22.77±10.78, 6.37±3.64 and 0.89±0.63 mm, respectively. For PEs which subtend <5% of lung tissue, the mean DSC is 0.79±0.08, with an average minimum Euclidean distance of 2.34±0.98 mm. Further MCP territory spatial correspondences regarding different levels of PE severity are detailed in *Figure 5* and *Table 3*.

Discussion

This study validated the MCP technique to quantify the tissue territory distal to PEs causing total occlusions using the resulting ischemic territory as the reference. An excellent correlation was shown between the MCP distal mass and REF ischemic territory mass with a near-unity slope and negligible bias. The results indicate that the MCP technique can accurately and automatically quantify the distal-PE territory corresponding to the pulmonary arterial obstruction using CTPA image data alone. Hence, this technique has the potential to provide more accurate assessment of PE-severity by quantifying the total mass of tissue at-risk caused by a PE.

Since CTPA enables direct visualization of pulmonary emboli in segmental and sub-segmental vessels, several CTPA indexes have previously been studied to quantify the severity of arterial obstruction (14-17). The Miller index was initially proposed, consisting of an objective arterial obstruction score and a subjective evaluation for peripheral perfusion reduction (15). Alternatively, the Walsh index calculates the number of segmental under-perfused vessels due to a PE in segmental or larger vessels, but is rarely used clinically due to computational complexity (16). Later, Qanadli *et al.* described a CT obstruction index with higher accuracy, which computes the severity of the proximal clot site based on the number of segmental branches arising distally combined with a weighting factor for the degree of obstruction (17). Yet, none of these CT-indices compute the mass of subtended tissue, where quantitative analysis of distal PEs in segmental and subsegmental branches may be of value (1,2). Fortunately, the MCP technique enables the assignment of each parenchymal voxel to its supplying vessel. Hence, the lung tissue distal to a pulmonary embolus can be delineated for better visualization and mass quantification, where the total PE-related tissue mass (or mass percent) can potentially play a role in improving PE risk stratification.

It is also important to consider that the distribution of ventilation and perfusion can be affected by a variety of lung diseases, such as the aforementioned PE, as well as chronic obstructive pulmonary disease, and lung cancer (31-33). As the lungs are anatomically and functionally separated into different lobes by lobar fissures, assessment of individual lung lobes is also of importance (34). Existing automatic lobe segmentation methods largely depend on the anatomy of healthy human lungs, including atlas-based (35,36), airway-guided (37), and deep learning-

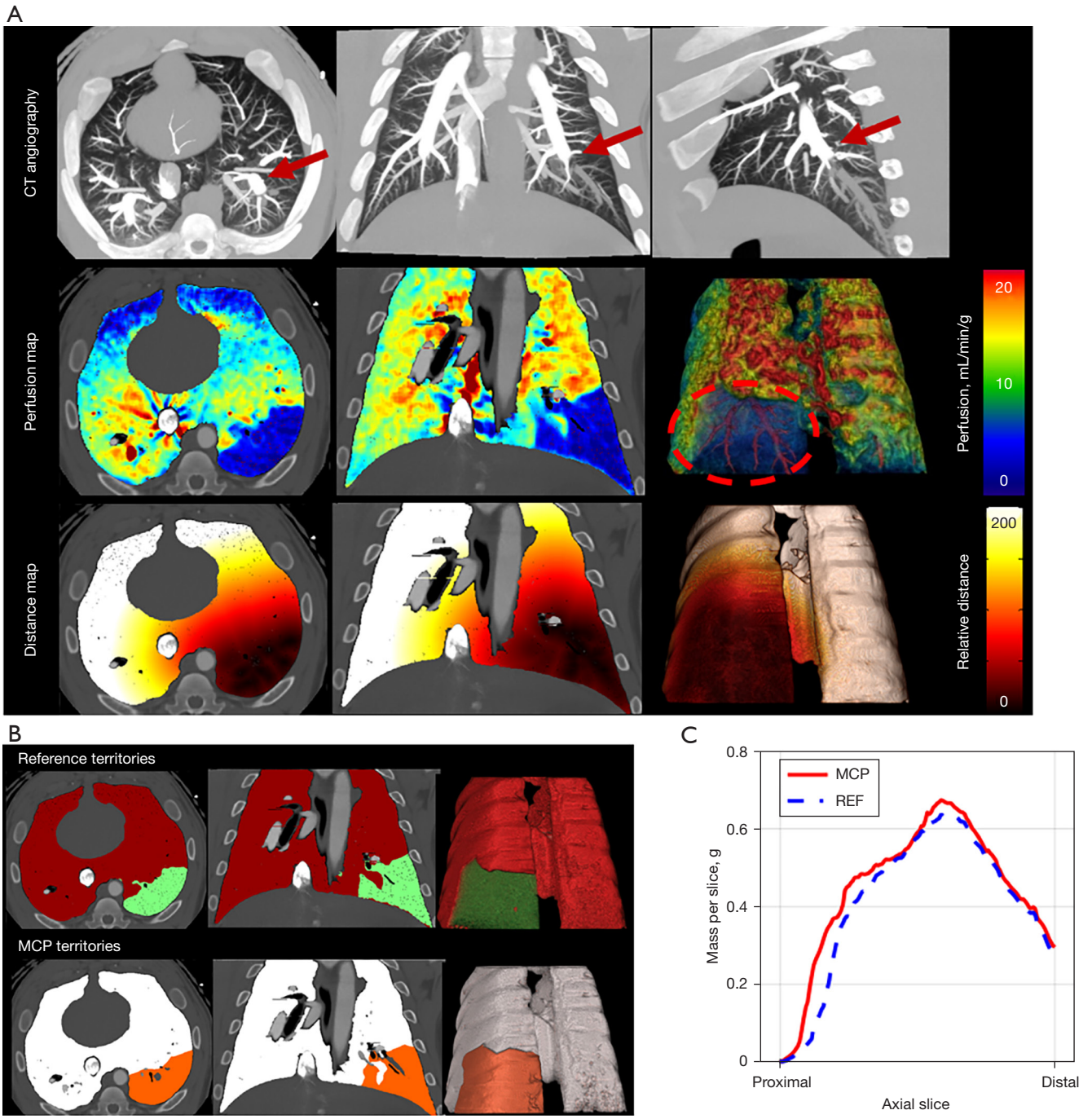

Figure 3 Qualitative results of the MCP and reference perfusion techniques. (A) The MIP of the CT angiography (top row), the perfusion distribution map (middle row), and the MCP distance map (bottom row). The red arrows shown in the CT angiography point to the balloon tip. The color bar shown in perfusion map indicates the perfusion in mL/min/g. The red dashed circle in the 3D perfusion map indicates the under-perfused lung tissue. The color bar shown in the MCP distance map indicates the relative distance of each voxel to its nearest distal vessel centerline point. (B) The MCP and reference standard territories are shown in axial, coronal and posterior 3D volumetric views. (C) Slice-by-slice comparison of PE-distal mass and ischemic tissue mass. CT, computed tomography; 3D, three-dimensional; MCP, minimum-cost path; MIP, maximum intensity projection; PE, pulmonary embolism; REF, reference standard.

Table 1 Comparisons of ischemic tissue mass and percent ischemic mass using the MCP and reference standard perfusion techniques

Animal ID	Number of acquisitions	Total lung mass (g)	Reference ischemic mass ($Mass_{REF}$) (g)	MCP ischemic mass ($Mass_{MCP}$) (g)	Reference ischemic mass-percent ($Percent_{REF}$) (g)	MCP ischemic mass-percent ($Percent_{MCP}$) (g)
Animal 1	6	429.2	16.3±7.5	17.2±7.9	3.8±1.8	4.0±1.8
Animal 2	7	469.7	70.3±20.6	75.6±22.4	15.0±4.4	16.1±4.78
Animal 3	4	496.0	101.1±34.0	100.8±42.8	20.4±6.9	20.3±8.6
Animal 4	3	409.8	39.9±44.1	34.9±40.7	9.8±10.8	8.5±9.9
Animal 5	5	483.7	33.6±27.7	35.5±29.6	6.9±5.7	7.3±6.1
Animal 6	3	372.5	69.7±1.3	85.4±5.8	18.7±1.1	22.9±1.5
Animal 7	7	481.2	20.1±1.9	19.1±0.1	4.2±0.4	4.0±0.1
Total	33	449.9±42.6	47.2±35.7	48.0±37.1	10.4±7.8	10.6±8.1

Data expressed as mean mass ± standard deviation or mean mass-percent ± standard deviation. MCP, Minimum-cost path technique; REF, reference standard perfusion technique.

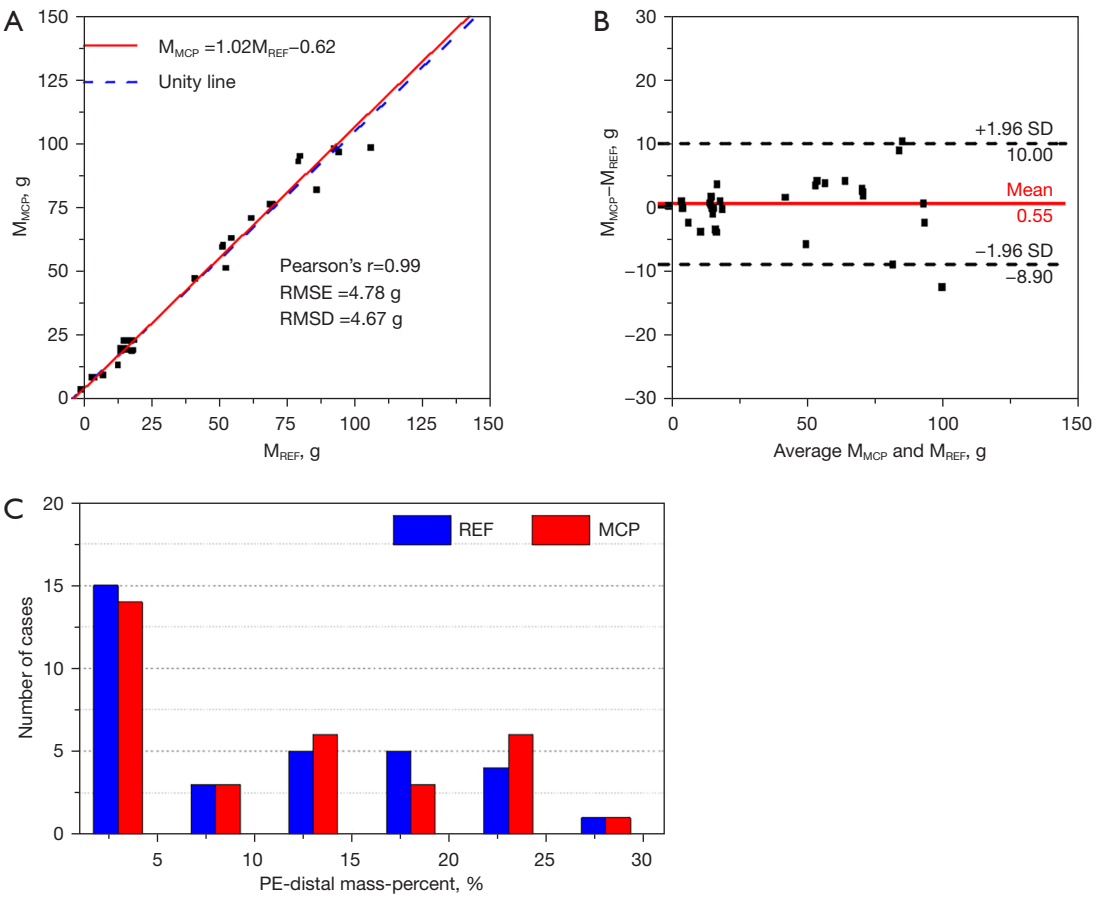

Figure 4 Mass correspondence comparison. (A) Linear regression and (B) Bland-Altman analysis comparing the MCP assigned PE-distal tissue masses (M_{MCP}) and the reference standard perfusion ischemic tissue masses (M_{REF}). (C) Histogram of the PE-distal mass-percent using the MCP and REF techniques on a total of 33 PE cases in this study. MCP, minimum-cost path; PE, pulmonary embolism; REF, reference standard; RMSE, root-mean-square error; RMSD, root-mean-square deviation; SD, standard deviation.

based algorithms (38). Unfortunately, these anatomical fissure-based lung lobe segmentation algorithms can be susceptible to anatomical variations, particularly in human lungs that may have incomplete fissures (39). Besides, as the deformation of lung anatomy may occur after coil treatment and lung volume reduction procedures, additional manual correction steps are required on the atlas to ensure accurate lobe segmentation for post-treatment CT analysis (33). Therefore, an automatic pulmonary lobar segmentation that does not rely on fissure visualization is needed to quantify the regional ventilation/perfusion and lung volume reduction. Fortunately, the MCP technique can also determine the lobar territories by assigning each voxel to its supplying vessel based on the shortest spatial distance, which is entirely independent of its borderlines or fissures. As the pulmonary arterial tree can be used for lobar assignment, such a technique can be robust over lung volume alteration or invisible fissures.

Table 2 Linear regression analysis of MCP and reference standard perfusion PE-distal masses

Variables	Values
Slope	1.02 [0.98, 1.08]
Intercept (g)	–0.62 [–3.76, 2.50]
Pearson's r	0.99 [0.98, 1.00]
Adj. R^2	0.98
CCC	0.97 [0.95, 0.99]
RMSE (g)	4.78
RMSD (g)	4.67
Paired *t*-test P value	0.51

For slope, intercept, CCC and Pearson's r, 95% CI are presented as [CI_{Lower}, CI_{Upper}]. P value less than 0.05 indicates significant difference. Adj. R^2, adjusted R^2; CCC, concordance correlation coefficient; CI, confidence interval; MCP, minimum-cost path; PE, pulmonary embolism; RMSE, root-mean-square error; RMSD, root-mean-square deviation.

Limitations

The present study has several limitations. First, the sample size of this animal study is relatively small, and the disease model generated is artificial. Further studies in a larger sample size of human subjects with real pulmonary pathology remains necessary. Second, the reference in this study was the ischemic territory derived from dynamic CT perfusion measurement. An alternative approach could have been a direct intravascular contrast injection right at a PE location in a pulmonary artery branch. Hence, any error in CT perfusion measurement may appear as an error in the MCP technique. Fortunately, a previous study has shown the accuracy of the two-volume first-pass CT perfusion measurement versus reference microsphere perfusion measurement (25). Third, only fully occluded PEs were assessed in this study while both partial and full occlusions occur clinically. Specifically, since the perfusion technique served as the REF, only total occlusions could be used to accurately demarcate the subtended area (based on low absolute perfusion values) for validation. Nevertheless, now that the MCP technique is validated, as long as the arterial centerlines can be extracted, the algorithm should

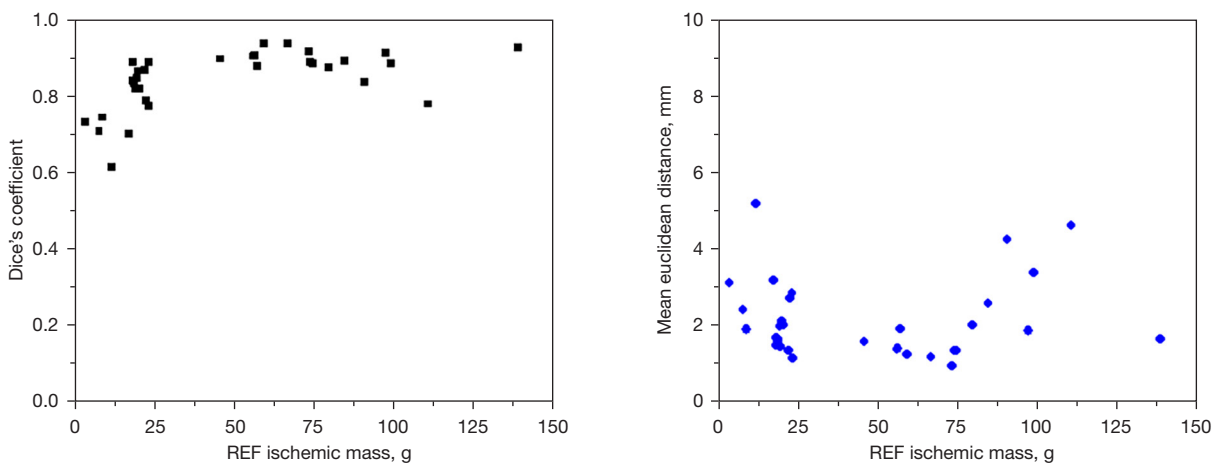

Figure 5 Dice's similarity coefficient and the mean Euclidean distance on the reference standard ischemic mass. REF, reference standard.

Table 3 Spatial correspondences of MCP and reference standard territories in the PE-distal territory

REF distal mass-percent (MP, %)	DSC	AD (mm)	MD (mm)	90th percentile distance (mm)	50th percentile distance (mm)
MP <5	0.79±0.08	2.34±0.98	26.15±7.94	6.80±3.28	1.28±0.52
5≤ MP <10	0.88±0.02	1.36±0.22	10.17±5.94	3.81±0.65	0.67±0.58
10≤ MP <15	0.91±0.03	1.43±0.29	15.11±3.42	4.69±0.83	0.30±0.48
15≤ MP <20	0.90±0.02	1.76±0.63	24.60±12.78	4.59±1.47	0.13±0.56
MP ≥20	0.86±0.06	3.06±1.49	31.63±13.61	10.38±5.14	0.94±0.61
All	0.84±0.08	2.12±1.03	22.77±10.78	6.37±3.64	0.89±0.63

Data expressed as mean ± standard deviation. REF, reference standard; MP, distal mass-percent; DSC, Dice similarity coefficient; AD, average distance; MD, maximum distance; MCP, minimum-cost path; PE, pulmonary embolism.

still be able to quantify the territory distal to suspected PE, regardless of partial or total occlusion. Fourth, the PE-distal mass-percent has not yet been compared with currently existing obstructive indices and risk factors, such as the pulmonary arterial pressure and right ventricular function. Hence, future studies should determine whether the mass-percent of the distal territory may enhance the predictive power of currently existing PE risk stratification indices. Finally, the vessel-specific assignment for lobar segmentation has not yet been quantitatively validated in this study.

Practical application

The minimum-cost path technique was validated by correlating the location of pulmonary emboli to the corresponding under-perfused tissue and potentially improving the stratification of pulmonary embolism severity. The quantification of subtended lung tissue distal to a PE using CTPA could help to determine the most appropriate individualized management approach.

Conclusions

The assignment technique was validated in a swine animal model showing that it was accurate. The technique enables an accurate assessment of lung tissue at risk distal to a pulmonary embolism using CT pulmonary angiography. This technique can potentially be used to quantify the fraction of lung tissue at risk distal to a pulmonary embolism to further improve the risk stratification of pulmonary embolism.

Acknowledgments

This study was part of the Ph.D. dissertation of Yixiao Zhao.

Funding: This study was supported, in part, by the Department of Radiological Sciences at the University of California, Irvine and a grant from Canon America Medical Systems.

Footnote

Conflicts of Interest: All authors have completed the ICMJE uniform disclosure form (available at https://qims.amegroups.com/article/view/10.21037/qims-22-791/coif). S Molloi has previously received grants from Canon America Medical Systems. The other authors have no conflicts of interest to declare

Ethical Statement: The authors are accountable for all aspects of the work in ensuring that questions related to the accuracy or integrity of any part of the work are appropriately investigated and resolved. The study was performed under a project protocol (No. AUP-18-191) granted by the Animal Care & Use Committee (IACUC), in compliance with institutional guidelines for the care and use of animals.

References

1. Essien EO, Rali P, Mathai SC. Pulmonary Embolism. Med Clin North Am 2019;103:549-64.
2. Wiener R, Schwartz LM, Woloshin S. Time Trends In Pulmonary Embolism In The United States: Evidence Of Overdiagnosis? In: D14 INNOVATIVE HEALTH SERVICES RESEARCH TO IMPROVE OUTCOMES [Internet]. American Thoracic Society; 2010 [cited 2021 Jul 16]. p. A5348–A5348. Available online: http://www.atsjournals.org/doi/abs/10.1164/ajrccm-conference.2010.181.1_MeetingAbstracts.A5348
3. Beckman MG, Hooper WC, Critchley SE, Ortel TL. Venous thromboembolism: a public health concern. Am J Prev Med 2010;38:S495-501.
4. Doğan H, de Roos A, Geleijins J, Huisman MV, Kroft LJ. The role of computed tomography in the diagnosis of acute and chronic pulmonary embolism. Diagn Interv Radiol 2015;21:307-16.
5. van der Hulle T, Cheung WY, Kooij S, Beenen LFM, van Bemmel T, van Es J, et al. Simplified diagnostic management of suspected pulmonary embolism (the YEARS study): a prospective, multicentre, cohort study. Lancet 2017;390:289-97.
6. Stein PD, Kayali F, Olson RE. Trends in the use of diagnostic imaging in patients hospitalized with acute pulmonary embolism. Am J Cardiol 2004;93:1316-7.
7. Weiss CR, Scatarige JC, Diette GB, Haponik EF, Merriman B, Fishman EK. CT pulmonary angiography is the first-line imaging test for acute pulmonary embolism: a survey of US clinicians. Acad Radiol 2006;13:434-46.
8. Corrigan D, Prucnal C, Kabrhel C. Pulmonary embolism: the diagnosis, risk-stratification, treatment and disposition of emergency department patients. Clin Exp Emerg Med 2016;3:117-25.
9. Carrier M, Righini M, Le Gal G. Symptomatic subsegmental pulmonary embolism: what is the next step? J Thromb Haemost 2012;10:1486-90.
10. Pesavento R, de Conti G, Minotto I, Filippi L, Mongiat M, de Faveri D, Maurizi F, Dalla Valle F, Piovella C, Pagnan A, Prandoni P; TACEP study. The value of 64-detector row computed tomography for the exclusion of pulmonary embolism. Thromb Haemost 2011;105:901-7.
11. Carrier M, Klok FA. Symptomatic subsegmental pulmonary embolism: to treat or not to treat? Hematology Am Soc Hematol Educ Program 2017;2017:237-41.
12. Simonneau G, Torbicki A, Dorfmüller P, Kim N. The pathophysiology of chronic thromboembolic pulmonary hypertension. Eur Respir Rev 2017;26:160112.
13. Lang IM, Dorfmüller P, Vonk Noordegraaf A. The Pathobiology of Chronic Thromboembolic Pulmonary Hypertension. Ann Am Thorac Soc 2016;13 Suppl 3:S215-21.
14. Stein PD. Quantification of pulmonary embolism by conventional and CT angiography. In: Pulmonary Embolism. Chichester, UK: John Wiley & Sons, Ltd., 2016:440-1.
15. Miller GA, Sutton GC, Kerr IH, Gibson RV, Honey M. Comparison of streptokinase and heparin in treatment of isolated acute massive pulmonary embolism. Br Med J 1971;2:681-4.
16. Wu AS, Pezzullo JA, Cronan JJ, Hou DD, Mayo-Smith WW. CT pulmonary angiography: quantification of pulmonary embolus as a predictor of patient outcome--initial experience. Radiology 2004;230:831-5.
17. Qanadli SD, El Hajjam M, Vieillard-Baron A, Joseph T, Mesurolle B, Oliva VL, Barré O, Bruckert F, Dubourg O, Lacombe P. New CT index to quantify arterial obstruction in pulmonary embolism: comparison with angiographic index and echocardiography. AJR Am J Roentgenol 2001;176:1415-20.
18. Kjaergaard J, Schaadt BK, Lund JO, Hassager C. Quantification of right ventricular function in acute pulmonary embolism: relation to extent of pulmonary perfusion defects. Eur J Echocardiogr 2008;9:641-5.
19. Çildag MB, Gok M, Karaman CZ. Pulmonary Artery Obstruction Index and Right Ventricular Dysfunction Signs in Initial and Follow up Pulmonary Computed Tomography Angiography in Acute Pulmonary Embolism. J Clin Diagn Res 2017;11:TC21-5.
20. Yu T, Yuan M, Zhang Q, Shi H, Wang D. Evaluation of computed tomography obstruction index in guiding therapeutic decisions and monitoring percutanous catheter fragmentation in massive pulmonary embolism. J Biomed Res 2011;25:431-7.
21. Malkasian S, Hubbard L, Dertli B, Kwon J, Molloi S. Quantification of vessel-specific coronary perfusion territories using minimum-cost path assignment and computed tomography angiography: Validation in a swine model. J Cardiovasc Comput Tomogr 2018;12:425-35.
22. Malkasian S, Hubbard L, Abbona P, Dertli B, Kwon J,

Molloi S. Vessel-specific coronary perfusion territories using a CT angiogram with a minimum cost path technique and its direct comparison to the American Heart Association 17-segment model. Eur Radiol 2020;30:3334-45.
23. Yuan SY, Rigor RR. 2010.
24. Sethian JA. A fast marching level set method for monotonically advancing fronts. Proc Natl Acad Sci U S A 1996;93:1591-5.
25. Zhao Y, Hubbard L, Malkasian S, Abbona P, Molloi S. Dynamic pulmonary CT perfusion using first-pass analysis technique with only two volume scans: Validation in a swine model. PLoS One 2020;15:e0228110.
26. Taha AA, Hanbury A. Metrics for evaluating 3D medical image segmentation: analysis, selection, and tool. BMC Med Imaging 2015;15:29.
27. Fenster A, Chiu B. Evaluation of Segmentation algorithms for Medical Imaging. Conf Proc IEEE Eng Med Biol Soc 2005;2005:7186-9.
28. Zou KH, Warfield SK, Bharatha A, Tempany CM, Kaus MR, Haker SJ, Wells WM 3rd, Jolesz FA, Kikinis R. Statistical validation of image segmentation quality based on a spatial overlap index. Acad Radiol 2004;11:178-89.
29. Cárdenes R, de Luis-García R, Bach-Cuadra M. A multidimensional segmentation evaluation for medical image data. Comput Methods Programs Biomed 2009;96:108-24.
30. Lin LI. A concordance correlation coefficient to evaluate reproducibility. Biometrics 1989;45:255-68.
31. Singh R, Nie RZ, Homayounieh F, Schmidt B, Flohr T, Kalra MK. Quantitative lobar pulmonary perfusion assessment on dual-energy CT pulmonary angiography: applications in pulmonary embolism. Eur Radiol 2020;30:2535-42.
32. Borges JB, Suarez-Sipmann F, Bohm SH, Tusman G, Melo A, Maripuu E, Sandström M, Park M, Costa EL, Hedenstierna G, Amato M. Regional lung perfusion estimated by electrical impedance tomography in a piglet model of lung collapse. J Appl Physiol (1985) 2012;112:225-36.
33. Shen M, Tenda ED, McNulty W, Garner J, Robbie H, Luzzi V, Aboelhassan AM, Van Geffen WH, Kemp SV, Ridge C, Devaraj A, Shah PL, Yang GZ. Quantitative Evaluation of Lobar Pulmonary Function of Emphysema Patients with Endobronchial Coils. Respiration 2019;98:70-81.
34. Doel T, Gavaghan DJ, Grau V. Review of automatic pulmonary lobe segmentation methods from CT. Comput Med Imaging Graph 2015;40:13-29.
35. Zhang L, Hoffman EA, Reinhardt JM. Atlas-driven lung lobe segmentation in volumetric X-ray CT images. IEEE Trans Med Imaging 2006;25:1-16.
36. van Rikxoort EM, Prokop M, de Hoop B, Viergever MA, Pluim JP, van Ginneken B. Automatic segmentation of pulmonary lobes robust against incomplete fissures. IEEE Trans Med Imaging 2010;29:1286-96.
37. Lassen B, van Rikxoort EM, Schmidt M, Kerkstra S, van Ginneken B, Kuhnigk JM. Automatic segmentation of the pulmonary lobes from chest CT scans based on fissures, vessels, and bronchi. IEEE Trans Med Imaging 2013;32:210-22.
38. Park J, Yun J, Kim N, Park B, Cho Y, Park HJ, Song M, Lee M, Seo JB. Fully Automated Lung Lobe Segmentation in Volumetric Chest CT with 3D U-Net: Validation with Intra- and Extra-Datasets. J Digit Imaging 2020;33:221-30.
39. Thapa P, Desai SP. Morphological variation of human lung fissures and lobes: An anatomical cadaveric study in North Karnataka, India. Indian J Health Sci Biomed Res 2016;9:284-7.

Cite this article as: Zhao Y, Malkasian S, Hubbard L, Molloi S. Validation of an automated technique for quantification of pulmonary perfusion territories using computed tomography angiography. Quant Imaging Med Surg 2023;13(5):3115-3126. doi: 10.21037/qims-22-791

